

RESTRICTED

UNCLASSIFIED

Copy 7  
RM L9E24

NACA RM L9E24



# RESEARCH MEMORANDUM

INVESTIGATION OF LOW-SPEED AILERON CONTROL CHARACTERISTICS  
AT A REYNOLDS NUMBER OF 6,800,000 OF A WING WITH  
LEADING EDGE SWEPT BACK 42° WITH AND  
WITHOUT HIGH-LIFT DEVICES

By

Thomas V. Bollech and George L. Pratt

Langley Aeronautical Laboratory  
Langley Air Force Base, Va.

CLASSIFIED DOCUMENT

This document contains classified information affecting the National Defense of the United States within the meaning of the Espionage Act, 18 USC 793 and 794. Its transmission or the revelation of its contents in any manner to an unauthorized person is prohibited by law. Information so classified may be imparted only to persons in the military and naval services of the United States, appropriate civilian officers and employees of the Federal Government who have a legitimate interest therein, and to United States citizens of known loyalty and discretion who of necessity must be informed thereof.

CLASSIFICATION CANCELLED

Auth: J.W. Crowley  
Date 12/7/53  
By E.O. 10574  
22-27A-12-18/53  
R7-1639  
Langley

## NATIONAL ADVISORY COMMITTEE FOR AERONAUTICS

WASHINGTON  
July 19, 1949

UNCLASSIFIED

RESTRICTED



UNCLASSIFIED

## NATIONAL ADVISORY COMMITTEE FOR AERONAUTICS

## RESEARCH MEMORANDUM

## INVESTIGATION OF LOW-SPEED AILERON CONTROL CHARACTERISTICS

AT A REYNOLDS NUMBER OF 6,800,000 OF A WING WITH

LEADING EDGE SWEPT BACK  $42^\circ$  WITH AND

WITHOUT HIGH-LIFT DEVICES

By Thomas V. Bollech and George L. Pratt

## SUMMARY

An investigation has been carried out at a Reynolds number of 6,800,000 to determine the low-speed lateral control characteristics of a 20-percent-chord half-span outboard aileron on a wing swept back  $42^\circ$  at the leading edge. The wing incorporated NACA 64<sub>1</sub>-112 airfoil sections perpendicular to the 0.273 chord line and had an aspect ratio of 4.01 and a taper ratio of 0.625.

The lateral control, aileron hinge-moment, aileron load, and balance-chamber-pressure characteristics were determined for the wing with and without high-lift and stall-control devices for an angle-of-attack range from  $-4^\circ$  through the stall.

The results of the investigation indicate that at low total aileron deflections the rolling moments produced were not influenced by model configuration. At large total aileron deflections ( $50^\circ$ ), lower values of rolling moments throughout the angle-of-attack range were obtained for the flap-deflected conditions than for the plain wing because of the loss in effectiveness of the downgoing aileron.

For a total aileron deflection of  $50^\circ$ , longitudinal trim changes were obtained for the flap-deflected conditions which would require a small degree of elevator travel to balance.

The rate of change in aileron hinge moment with deflection in a steady roll  $C_{hs}$  of the unbalanced aileron was approximately constant in the low angle-of-attack range and decreased appreciably in the higher angle-of-attack range for the plain wing and for the wing with leading- and trailing-edge flaps deflected. The addition of fences to the flapped configuration resulted in a more constant variation of  $C_{hs}$  with angle of attack. Accordingly, only for the latter case was the

~~RESTRICTED~~

UNCLASSIFIED

aerodynamic-balance requirement essentially constant throughout the angle-of-attack range.

The calculated value of the rolling-effectiveness parameter for the plain wing at zero angle of attack agreed within 2 percent with the experimental value.

## INTRODUCTION

One of the many low-speed problems associated with the use of highly swept wings is the difficulty in providing adequate lateral control, particularly in the region of maximum lift. Present-day experimental data on the aileron lateral control characteristics of swept wings are largely limited to low-scale results such as reported in reference 1. In order to provide data at high Reynolds numbers, an investigation of the low-speed aileron control characteristics of swept wings has been undertaken in the Langley 19-foot pressure tunnel. As a part of the lateral-control investigation at large scale, the aileron control characteristics of a  $42^\circ$  sweptback wing incorporating circular-arc sections and of a  $37^\circ$  sweptback wing incorporating NACA 64<sub>1</sub>-212 sections have been presented in references 2 and 3, respectively.

The lateral control characteristics for a  $42^\circ$  sweptback wing fitted with a 20-percent-chord half-span outboard aileron are presented in this paper. The wing incorporated NACA 64<sub>1</sub>-112 sections perpendicular to the 0.273 chord line and had an aspect ratio of 4.01 and taper ratio of 0.625. The aileron lateral control characteristics are presented together with the aileron load characteristics and balance-chamber pressures for the plain wing and for the wing equipped with high-lift and stall-control devices. These devices included extensible round-nose leading-edge flaps, trailing-edge split flaps, and upper-surface fences.

The investigation was carried out at a Reynolds number of 6,800,000, and a Mach number of approximately 0.16 for an angle-of-attack range from  $-4^\circ$  through the stall.

## SYMBOLS

All data are referred to a system of axes (wind axes) originating in the plane of symmetry at the quarter-chord point of the mean aerodynamic chord. The symbols used herein are defined as follows:

$C_L$	lift coefficient $\left( \frac{\text{Lift}}{qS} \right)$
$C_m$	pitching-moment coefficient $\left( \frac{\text{Pitching moment}}{qSc} \right)$
$C_n$	yawing-moment coefficient $\left( \frac{\text{Yawing moment}}{qSb} \right)$
$C_l$	rolling-moment coefficient $\left( \frac{\text{Rolling moment}}{qSb} \right)$
$C_{Z_a}$	aileron load coefficient, positive in up direction $\left( \frac{\text{Aileron load measured perpendicular to wing chord line}}{qS_a} \right)$
$C_{h_a}$	aileron hinge-moment coefficient $\left( \frac{\text{Aileron hinge moment}}{qM_a} \right)$
$P_R$	resultant aileron balance-chamber-pressure coefficient $\left( \frac{\text{Pressure below seal} - \text{Pressure above seal}}{q} \right)$
$E$	aileron-seal leakage factor $\left( 1 - \frac{\text{Pressure difference across seal}}{\text{Pressure difference across vents}} \right)$
$q$	free-stream dynamic pressure, pounds per square foot $\left( \frac{1}{2} \rho V^2 \right)$
$b$	wing span measured perpendicular to plane of symmetry, feet
$\rho$	mass density, slugs per cubic foot
$V$	free-stream velocity, feet per second

$M_a$	twice moment area of aileron measured behind aileron hinge line, cubic feet $\left( \int_{0.5b/2}^{0.975b/2} c'_a{}^2 dy \right)$
$S$	wing area, square feet
$S_a$	aileron area behind hinge line, square feet
$\bar{c}$	wing mean aerodynamic chord measured parallel to plane of symmetry $\left( \frac{2}{S} \int_0^{b/2} c^2 dy \right)$
$c_a$	root-mean-square chord of aileron measured normal to aileron hinge line, feet
$c'_a$	local aileron chord measured perpendicular to aileron hinge line
$c$	local wing chord measured parallel to plane of symmetry, feet
$c'$	local wing chord measured perpendicular to 0.273 chord line, feet
$\bar{c}_b$	root-mean-square chord of hypothetical aileron balance measured ahead of and normal to aileron hinge line, feet
$\Lambda$	sweep angle of wing leading edge, degrees
$y$	spanwise coordinate, feet
$\alpha$	angle of attack, degrees
$\delta_a$	aileron deflection, measured perpendicular to the aileron hinge line, degrees
$\delta_{a_{total}}$	arithmetical sum of equal up and down aileron deflections for an assumed set of ailerons
$C_{l\delta}$	rate of change of rolling-moment coefficient with aileron deflection
$C_{h\delta}$	rate of change of aileron hinge-moment coefficient with aileron deflection

$C_{h\alpha}$	rate of change of aileron hinge-moment coefficient with angle of attack
$P_{R\delta}$	rate of change of aileron balance-chamber-pressure coefficient with aileron deflection
$P_{R\alpha}$	rate of change of aileron balance-chamber-pressure coefficient with angle of attack
$C_{h\delta}$	rate of change of aileron hinge-moment coefficient in steady roll with aileron deflection

### MODEL AND TESTS

#### Model

The wing was constructed of laminated mahogany to the plan form shown in figure 1. The sweep angle of the leading edge was  $42.05^\circ$ , and the airfoil sections perpendicular to the 0.273 chord line were NACA 64<sub>1</sub>-112 sections. (The 0.273 chord line corresponds to the 0.25 chord line of the wing with unswept panels.) The aspect ratio of the wing was 4.01 and the taper ratio was 0.625. The wing tips were parabolic in plan form and elliptical in cross section. The wing was constructed with no geometric dihedral or twist.

The wing was fitted with a 0.20c' half-span outboard aileron installed on the left wing panel only. The aileron was of an internally sealed unbalanced type and had a flat-sided contour with a  $11.1^\circ$  trailing-edge angle measured perpendicular to the hinge line. The aileron hinge moments and aileron loads were measured by resistance-type electrical strain gages. The aileron seal was attached in such manner that moments and forces transmitted to the aileron were negligible. Except for cutouts to allow for the installation of strain gages, the seal extended the full span of the aileron. A total of 12 pressure orifices were installed in the balance chamber, six above and six below the seal to provide a measurement of the pressure differential across the seal. Details of the aileron are shown in figure 1.

The leading-edge flaps used in the investigation were of the round-nose extensible type with a constant chord of 3.19 inches and extended from 40 to 97.5 percent of the semispan. The deflection of the flaps was approximately  $50^\circ$  with respect to the section chord perpendicular to the 0.273 chord line.

Split flaps were used as the trailing-edge high-lift device in this investigation and had a chord of 20 percent of the wing chord measured perpendicular to the 0.273 chord line (which corresponds to 18.4 percent of the wing chord measured parallel to the plane of symmetry) and extended from the plane of symmetry to 50 percent of the semispan. The flaps were constructed of  $\frac{1}{16}$ -inch sheet steel and were attached to the wing at an angle of  $60^\circ$ . The angle between the flap chord line and the lower surface of the wing thereby constitutes the angle of flap deflection and is measured perpendicular to the 0.273 chord line.

The upper-surface fences were located at 50 percent of the wing semispan and were constructed of  $\frac{1}{16}$ -inch sheet steel cut to fit the upper surface of the wing. The fences extended from 5 percent of the local chord to the wing trailing edge. The height of the fences was arbitrarily set at 60 percent of the maximum thickness of the local airfoil section parallel to the plane of symmetry.

Details of the high-lift and stall-control devices are shown in figure 2.

#### Tests

The tests were conducted in the Langley 19-foot pressure tunnel with the model mounted in the tunnel as shown in figure 3. The air in the tunnel was compressed to approximately 0.0055 slugs per cubic foot enabling the tests to be made at a Reynolds number of 6,800,000 and a Mach number of 0.16.

The aileron lateral control characteristics and the wing lift, drag, and pitching-moment characteristics were determined for the plain wing and the wing equipped with high-lift and stall-control devices for an angle-of-attack range from  $-4^\circ$  through the stall and for an aileron-deflection range from  $-25^\circ$  to  $25^\circ$ .

#### REDUCTION OF DATA

All data have been reduced to nondimensional coefficient form. Corrections for support tare and interference have been applied to all force and moment data. Jet-boundary corrections determined by means of reference 4 and air-flow-misalignment corrections have been applied to the angle of attack and drag coefficient. In addition, a

jet-boundary correction has been applied to the pitching moment. Corrections for jet-boundary effects on rolling and yawing moments were found to be small and therefore have not been applied.

As previously stated, the aileron seal was not continuous along the span of the aileron due to the installation of the strain-gage beams. This discontinuity resulted in some degree of leakage across the seal. A calibration of the leakage through the aileron seal indicated a leakage factor  $E$  of 0.13. The resultant balance-chamber pressures presented herein have been corrected to a 100-percent sealed condition. No correction for the effects of leakage on the aileron hinge-moment and load characteristics have been made to the data since the amount of leakage (based on effective gap area defined in reference 5) was found to be very small, and the effects are believed to be negligible.

## RESULTS AND DISCUSSION

Lateral characteristics.— The aileron characteristics for the plain wing and the wing equipped with high-lift and stall-control devices are presented in figures 4 to 6. Attention is called to the fact that the rolling-moment coefficients for the plain wing are not faired beyond angles of attack near maximum lift. Beyond that point the lift curve levels off and, as a result of the varying degree of flow separation that existed on the wing at the high angles of attack, the rolling-moment data became very erratic. Yawing moments for intermediate aileron deflections have been omitted from figures 4 to 6 inasmuch as the variations were found to be small and can be assumed to be approximately linear through the range investigated.

Comparison of the rolling moments produced by equal up and down aileron deflections for various configurations (fig. 7) indicates that at low values of aileron deflections the rolling moment produced was not influenced by model configuration. At larger total aileron deflections ( $50^\circ$ ) the addition of high-lift and stall-control devices resulted in somewhat lower values of rolling moment throughout the angle-of-attack range and, as might be expected from the loss in rolling moment, also resulted in less adverse yawing moments than were obtained for the plain wing.

The variation of  $C_l$  with aileron deflection (fig. 8) (for the plain-wing condition) was approximately the same for corresponding positive and negative aileron deflections for all of the angles of attack investigated. On the other hand, with leading- and trailing-edge flaps deflected, the values of  $C_l$  for positive aileron

deflections were lower than those obtained for the corresponding negative deflections. This effect increased with angle of attack. The addition of upper-surface fences appeared to have little effect on improving the flap-deflected aileron effectiveness. The reduced aileron effectiveness at large positive aileron deflections for the wing with high-lift and stall controls deflected was noted in reference 2 where aileron tests were made on a wing of approximately the same plan form but incorporating biconvex airfoil sections. Comprehensive information from which an exact reason could be obtained for the loss in aileron effectiveness was not available; however, it may be due in part to the existence of some degree of flow separation in the region of the aileron as is indicated by the lift and moment characteristics obtained.

A comparison of the variation of  $C_{l\delta}$  with angle of attack for various model configurations (fig. 9) indicates that the values of  $C_{l\delta}$  (at  $\delta_a = 0^\circ$ ) were approximately the same for all model configurations investigated up to an angle of attack of approximately  $10^\circ$  where  $C_{l\delta}$  for the plain wing started to decrease. The value of  $C_{l\delta}$  for the wing with leading- and trailing-edge flaps deflected was slightly greater throughout the higher angle-of-attack range. For the condition with leading- and trailing-edge high-lift devices and upper-surface fences,  $C_{l\delta}$  started to decrease at an angle of attack of  $12^\circ$  and at an angle of attack of  $16^\circ$  was 50 percent lower than that obtained for the plain wing. The experimental value of  $C_{l\delta}$  obtained for the plain wing at zero angle of attack was 0.00105. A value of  $C_{l\delta}$  of 0.00103 was calculated for the same test condition by the method of reference 6 and is within 2 percent of the experimental value.

At zero angle of attack, favorable yawing moments were obtained for all model configurations (fig. 7); however, as the angle of attack was increased, the yawing moments for all configurations became adverse.

Pitching-moment characteristics.—The increments of pitching moment due to positive and negative aileron deflections were approximately equal for the plain wing but were unequal in the case of the wing with high-lift and stall-control devices deflected (figs. 4 to 6). As in the case of the rolling-moment characteristics, the large positive aileron deflections produced a smaller increment in pitching moment than corresponding negative deflections. Based upon the results of horizontal-tail tests of reference 7 and assuming that the elevator effectiveness would be 50 percent of the stabilizer effectiveness, it

is estimated that slightly less than  $2^\circ$  elevator travel would be necessary to counteract the pitching moment resulting from a total aileron deflection of  $50^\circ$  for the flap-deflected configurations throughout the angle-of-attack range.

Hinge-moment characteristics.— A representative plot of the variation of aileron hinge moment with aileron deflection is shown in figure 10. The effect of high-lift and stall-control devices on the aileron hinge-moment parameters,  $C_{h\delta}$ ,  $C_{h\alpha}$ ,  $P_{R\delta}$ , and  $P_{R\alpha}$ , is shown in figure 9. No appreciable effect on  $C_{h\delta}$  was noted when leading- and trailing-edge flaps were deflected; however, the high-lift devices caused a decrease in  $C_{h\alpha}$  in the higher angle-of-attack range. Except for very low angles of attack, the addition of leading- and trailing-edge flaps increased the value of  $P_{R\delta}$ . In the case of  $P_{R\alpha}$ , the addition of high-lift devices reduced the values of  $P_{R\alpha}$  in the higher angle-of-attack range and thereby reduced the abrupt increases in  $P_{R\alpha}$  obtained for the plain wing. In the lower angle-of-attack range the addition of flaps served to increase the values of  $P_{R\alpha}$ . The addition of upper-surface fences produced variations of the aileron hinge-moment parameters which were more uniform throughout the angle-of-attack range.

The variations of  $C_{h\alpha}$ ,  $C_{h\delta}$  with angle of attack for the various model configurations investigated are presented in figure 11. Large positive values of  $C_{h\alpha}/C_{h\delta}$  were obtained in the high angle-of-attack range for the plain wing and the wing equipped with leading- and trailing-edge flaps. The addition of upper-surface fences to the latter configuration greatly reduced the large values of  $C_{h\alpha}/C_{h\delta}$  obtained in the high angle-of-attack range.

Based upon the analysis of reference 8, values of  $C_{h\alpha}/C_{h\delta}$  in excess of 2.0 are likely to result in large values of the ratio of peak force obtained at the initiation of a roll to the steady force in the roll with the possibility of objectionably high stick forces during the rapid initiation and reversal of an aileron roll. It can be seen from figure 11 that for the plain wing and the wing equipped with leading- and trailing-edge flaps an analysis such as presented in reference 8 would be necessary to insure against the possibility of obtaining excessive stick forces in any particular design.

A possible high-speed flight arrangement may incorporate an aileron with a geared tab and no aerodynamic balance. Although this particular type of design may prove satisfactory in some instances, it should be pointed out that high positive values of  $C_{h\alpha}/C_{h\delta}$  are attained in practice through the use of this type of lateral-control arrangement. It is evident, therefore, that a geared-tab arrangement without aerodynamic balance would not prove satisfactory for this particular case, inasmuch as it would tend to aggravate the already large positive values of  $C_{h\alpha}/C_{h\delta}$ .

Another approach to the high-speed flight problem is to incorporate in the aileron design some degree of aerodynamic balance. In an effort to show the effect of an internally sealed aerodynamic balance on  $C_{h\delta}'$  (the rate of change of aileron hinge moment with deflection in a steady roll), some calculations by means of equations presented in reference 2 were made for various degrees of aerodynamic balance for the configurations investigated and are presented in figure 12. It can be seen that in the case of the plain wing, the degree of aerodynamic balance required for  $C_{h\delta}' = 0$  varies from approximately 45 percent of the aileron chord at  $\alpha = 0^\circ$  to 50 percent at  $\alpha = 16^\circ$ . With flaps deflected, the required aerodynamic balance varied from approximately 50 to 30 percent of the aileron chord for angles of attack of  $0^\circ$  and  $16^\circ$ , respectively. With upper-surface fences installed, the aerodynamic balance required was approximately 50 percent of the aileron chord throughout the angle-of-attack range.

Aileron load coefficients.— The aileron load coefficients are presented in figures 4 to 6 for the purpose of supplying design information on the aerodynamic forces that would be anticipated on a geometrical similar aileron. Due to the limitations of the strain-gage arrangement, it was not possible to measure the aileron drag forces parallel to the wing chord line and, therefore, no attempt was made to present true normal-force coefficients.

### CONCLUSIONS

From an investigation of the lateral control characteristics at a Reynolds number of 6,800,000 of a wing with the leading edge swept back  $42^\circ$  with and without high-lift devices, the following conclusions can be made:

1. At low total aileron deflections the rolling moments produced were not influenced by model configurations. At large total aileron deflections ( $50^\circ$ ), lower values of rolling moments throughout the

angle-of-attack range were obtained for the flap-deflected conditions than for the plain wing because of the loss in effectiveness of the downgoing aileron.

2. For a total aileron deflection of  $50^{\circ}$ , longitudinal trim changes were obtained for the flap-deflected conditions which would require a small degree of elevator travel to balance.

3. The hinge moment of the unbalanced aileron was approximately uniform in the low angle-of-attack range and decreased appreciably in the higher angle-of-attack range for the plain wing and for the wing with leading- and trailing-edge flaps deflected. The addition of fences to the flapped configuration resulted in a more uniform hinge-moment variation. Accordingly, only for the latter case was the aerodynamic-balance requirement essentially constant throughout the angle-of-attack range.

4. The calculated value of the rolling-effectiveness parameter for the plain wing at zero angle of attack agreed within 2 percent with the experimental value.

Langley Aeronautical Laboratory  
National Advisory Committee for Aeronautics  
Langley Air Force Base, Va.

## REFERENCES

1. Fischel, Jack, and Schneiter, Leslie E.: An Investigation at Low Speed of a  $51.3^\circ$  Sweptback Semispan Wing Equipped with 16.7-Percent-Chord Plain Flaps and Ailerons Having Various Spans and Three Trailing-Edge Angles. NACA RM L8E20, 1948.
2. Spooner, Stanley H., and Woods, Robert L.: Low-Speed Investigation of Aileron and Spoiler Characteristics of a Wing Having  $42^\circ$  Sweepback of the Leading Edge and Circular-Arc Airfoil Sections at Reynolds Numbers of Approximately  $6.0 \times 10^6$ . NACA RM L9A07, 1949.
3. Graham, Robert R., and Koven, William: Lateral-Control Investigation on a  $37^\circ$  Sweptback Wing of Aspect Ratio 6 at a Reynolds Number of 6,800,000. NACA RM L8K12, 1948.
4. Eisenstadt, Bertram J.: Boundary-Induced Upwash for Yawed and Swept-Back Wings in Closed Circular Wind Tunnels. NACA TN 1265, 1947.
5. Bird, J. D.: Effect of Leakage past Aileron Nose on Aerodynamic Characteristics of Plain and Internally Balanced Ailerons on NACA 66(215)-216,  $a = 1.0$  Airfoil. NACA ACR L5F13a, 1945.
6. Lowry, John G., and Schneiter, Leslie E.: Estimation of Effectiveness of Flap-Type Controls on Sweptback Wings. NACA TN 1674, 1948.
7. Spooner, Stanley H., and Martina, Albert P.: Longitudinal Stability Characteristics of a  $42^\circ$  Sweptback Wing and Tail Combination at a Reynolds Number of  $6.8 \times 10^6$ . NACA RM L8E12, 1948.
8. Morgan, M. B., and Bethwaite, C. F.: Notes on Stick Force Characteristics During the Initiation and Reversal of an Aileron Roll. R. & M. No. 1985, British A.R.C., 1943.

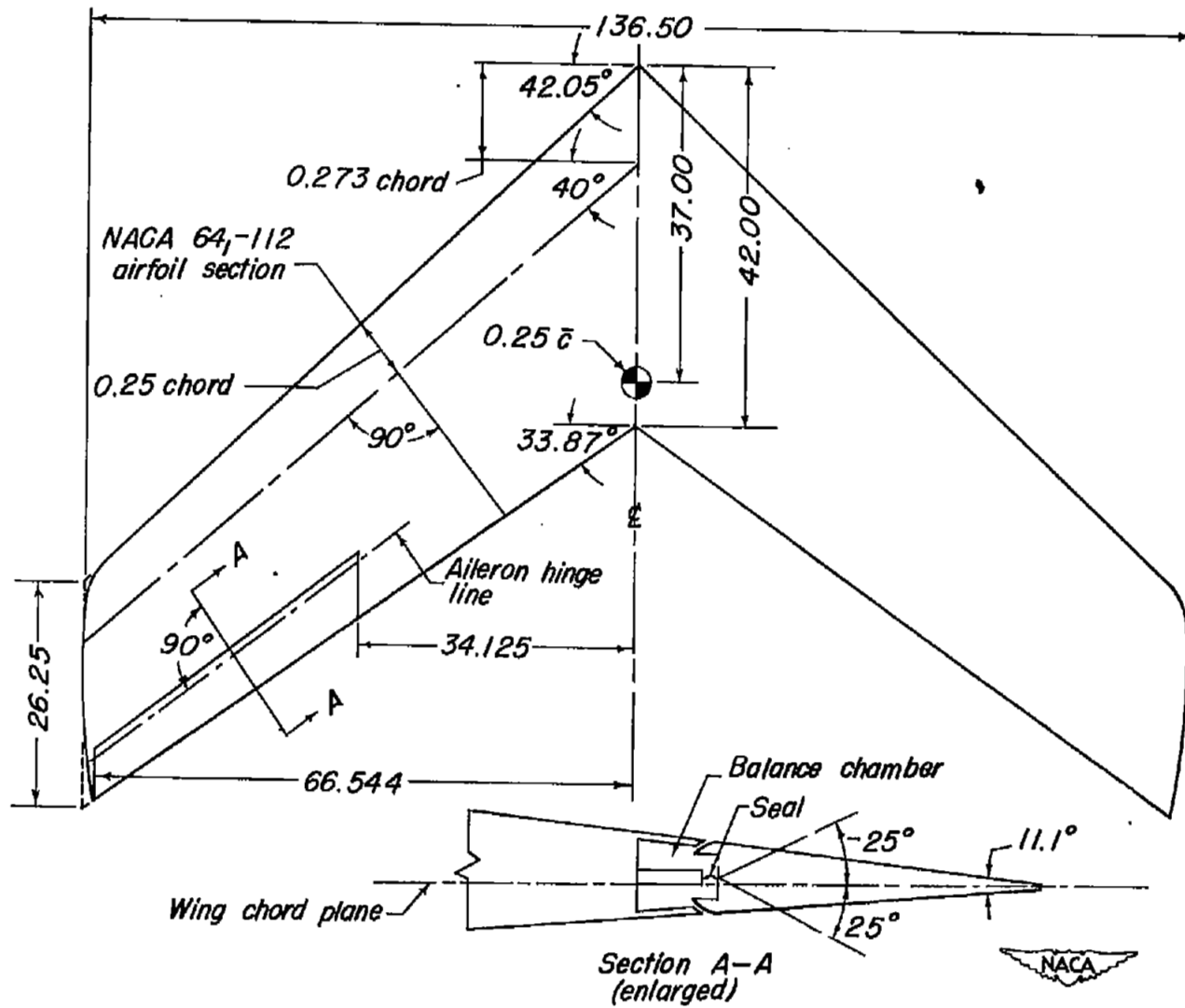


Figure 1.— Layout of 42° sweptback wing and aileron details. All dimensions in inches. Wing area, 32.24; aspect ratio, 4.01.

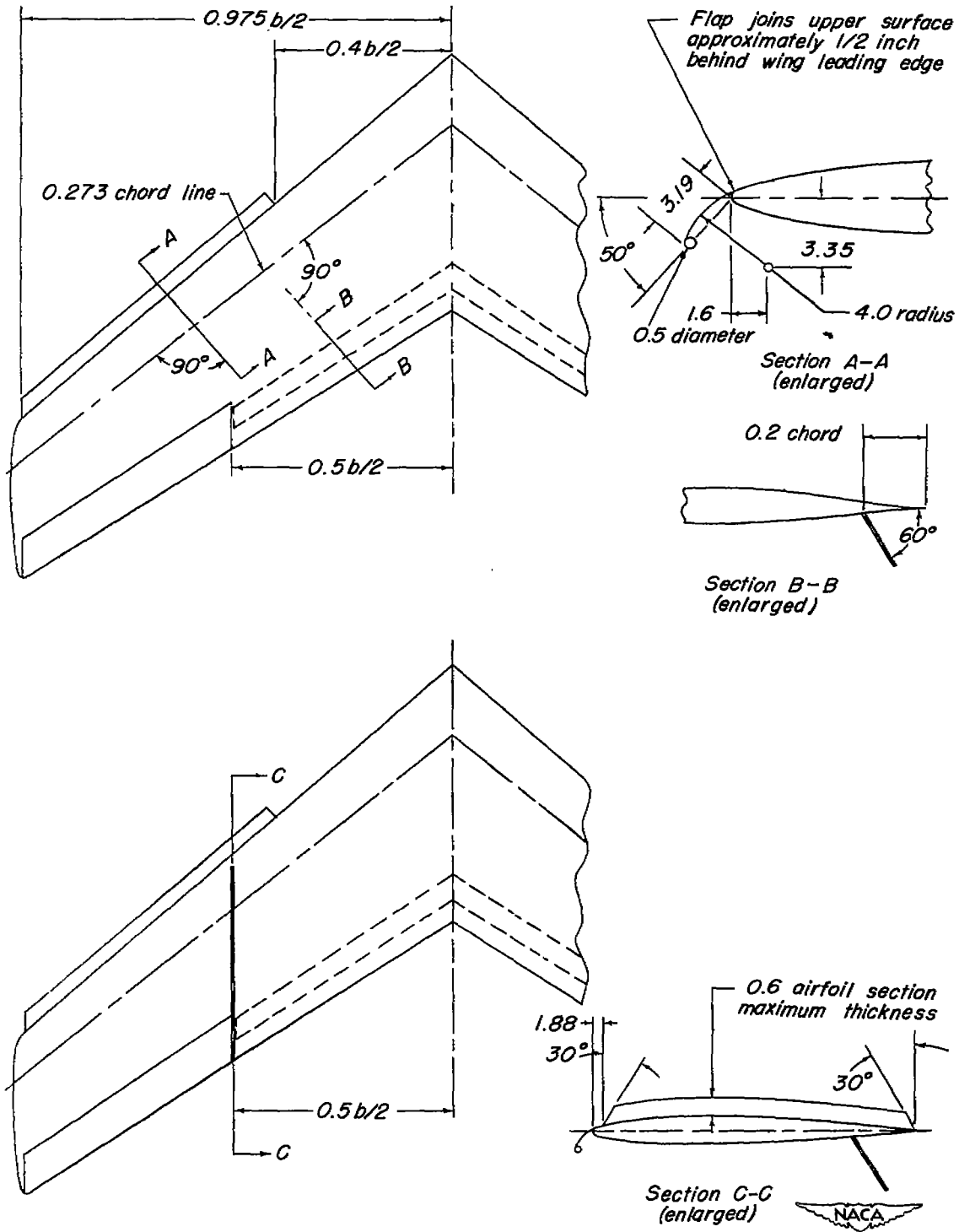


Figure 2.— Details of wing high-lift and stall-control devices.

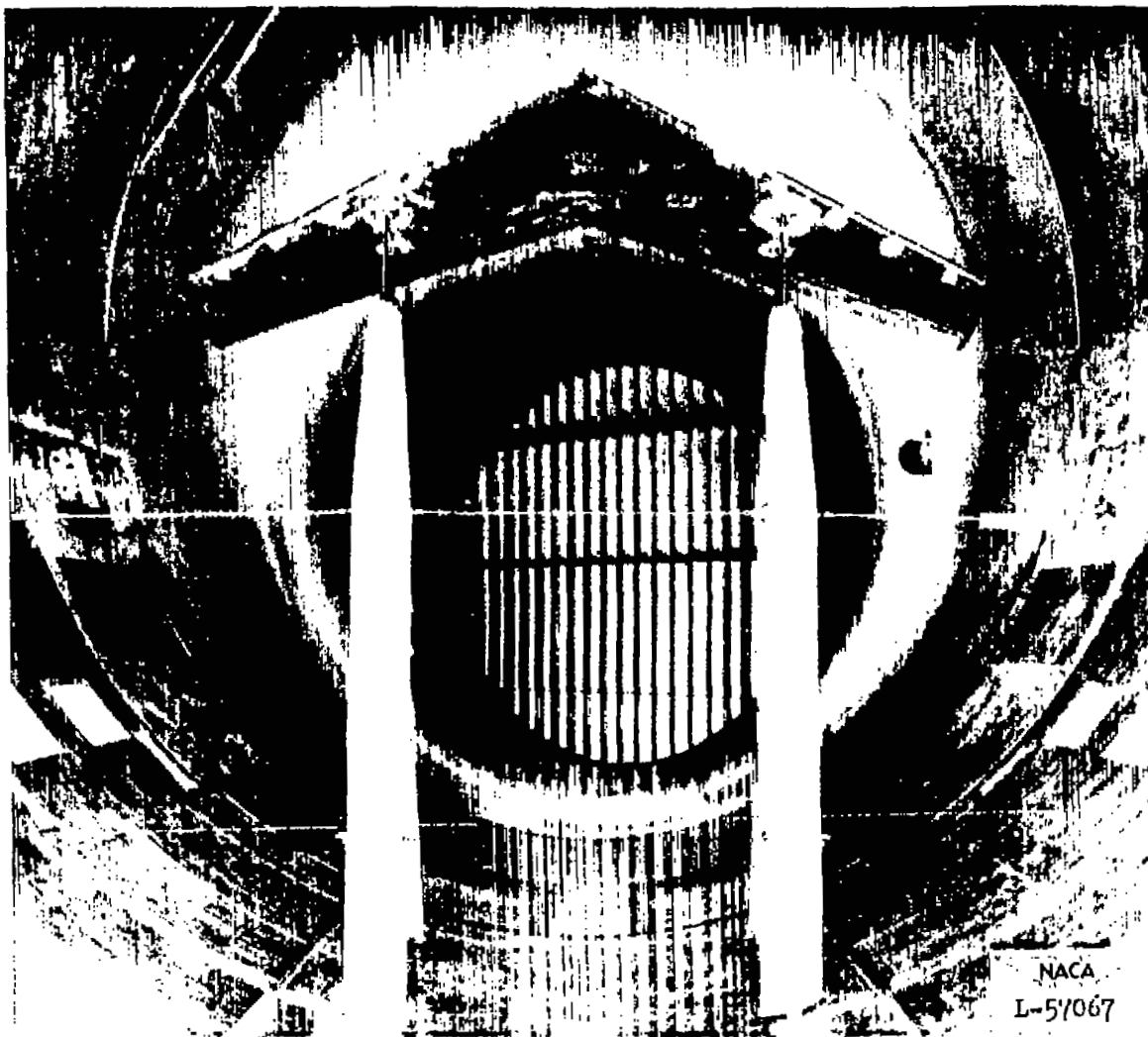
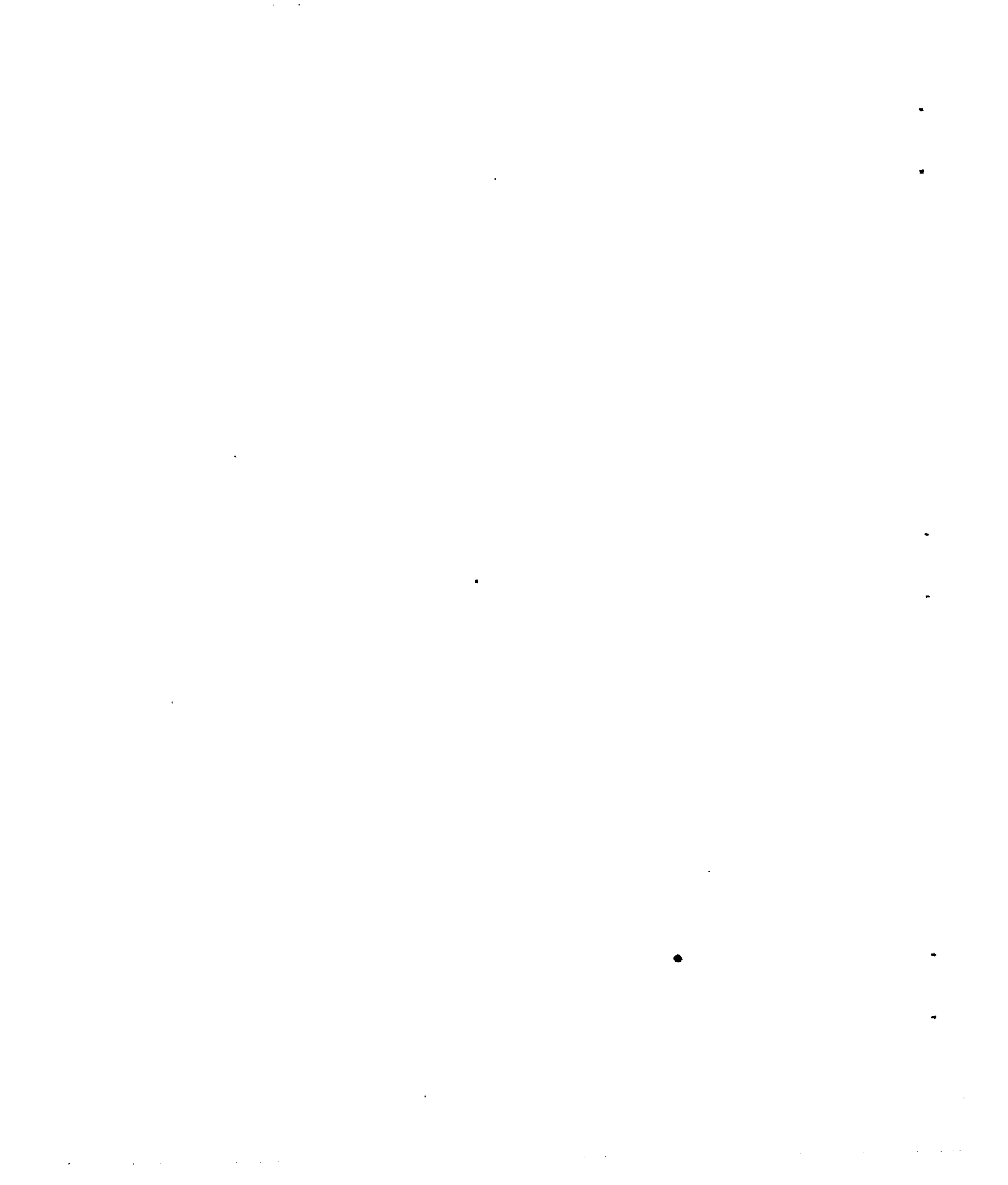
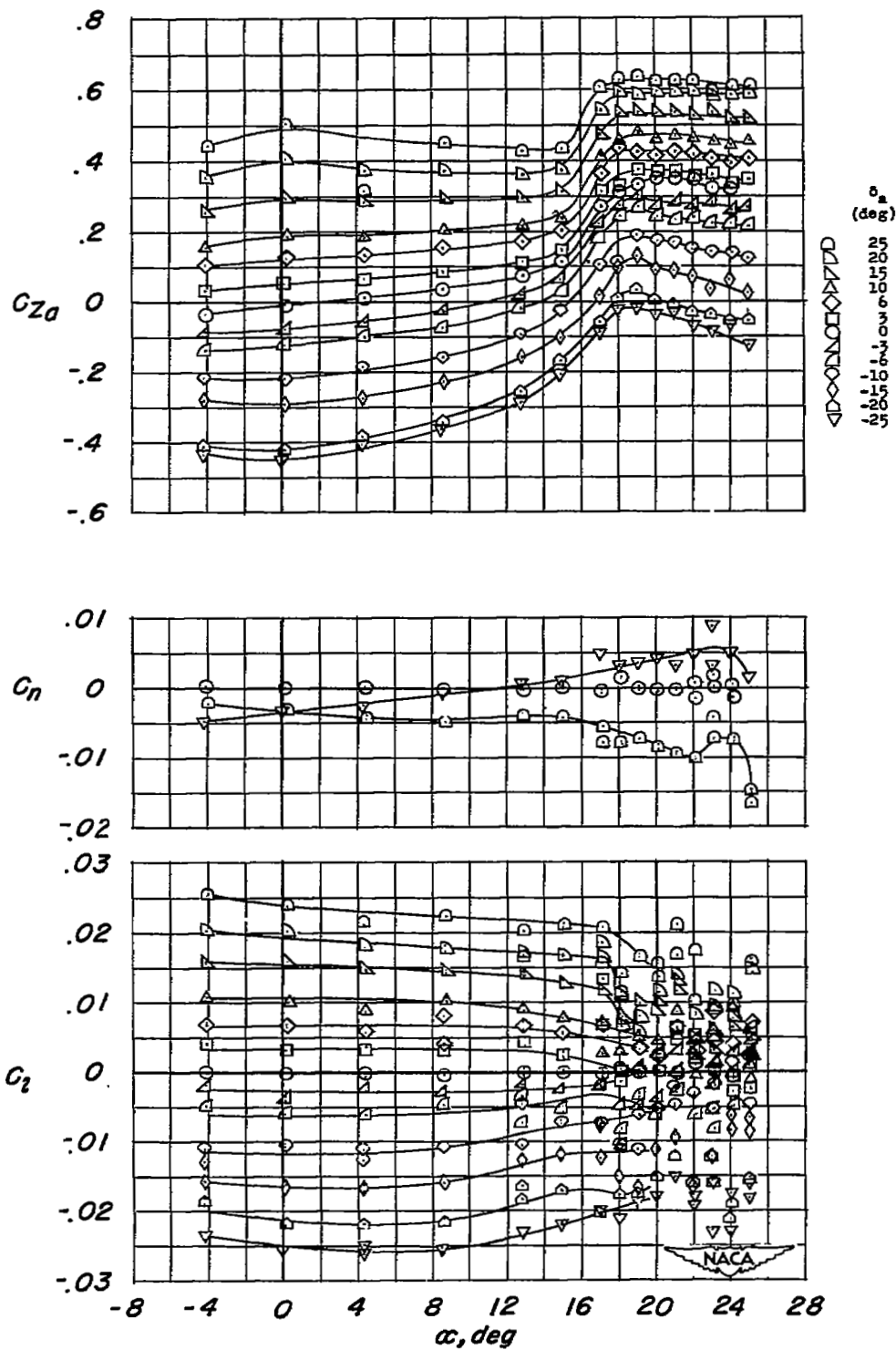


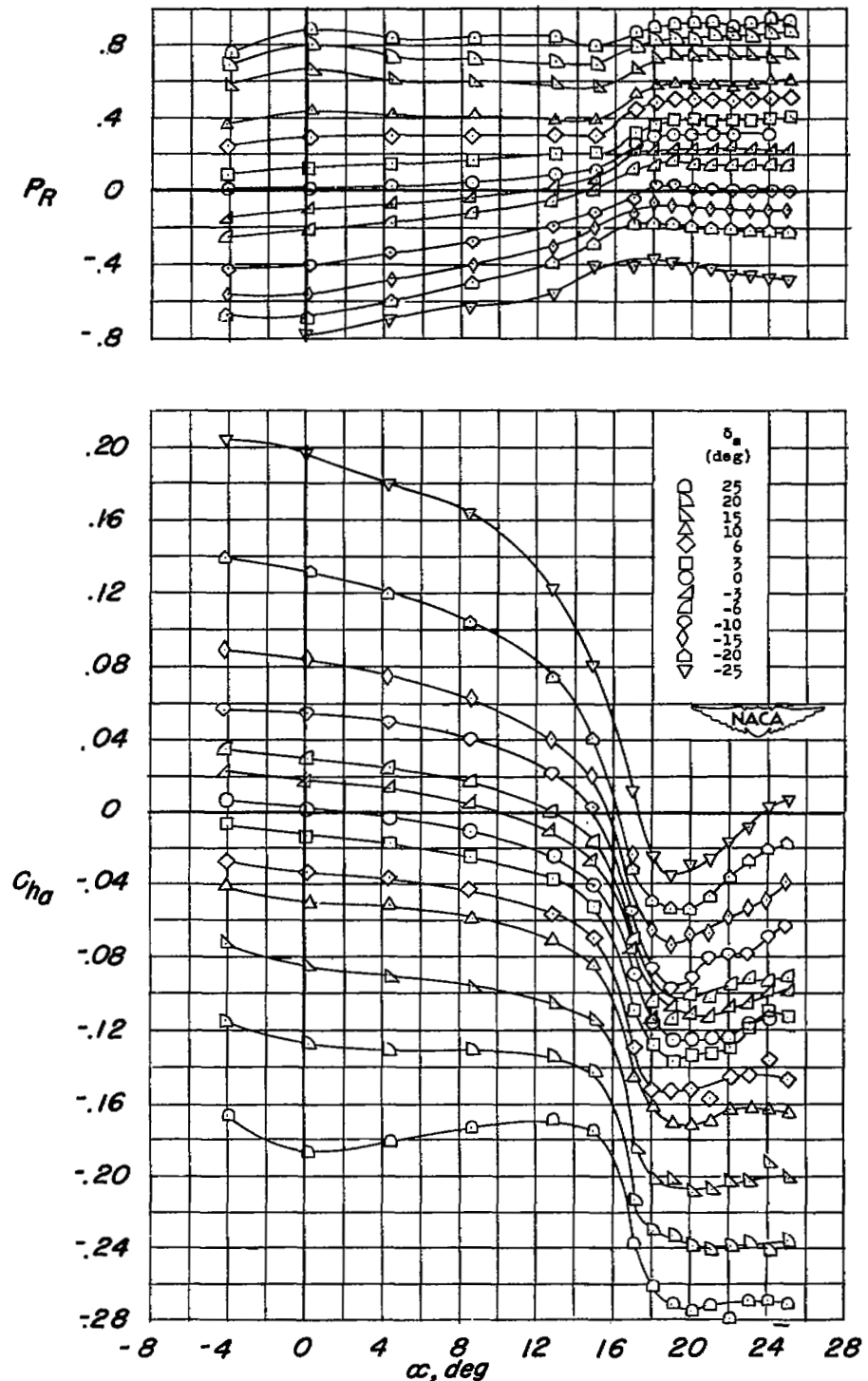
Figure 3.- The  $42^\circ$  sweptback wing mounted in the Langley 19-foot pressure tunnel.





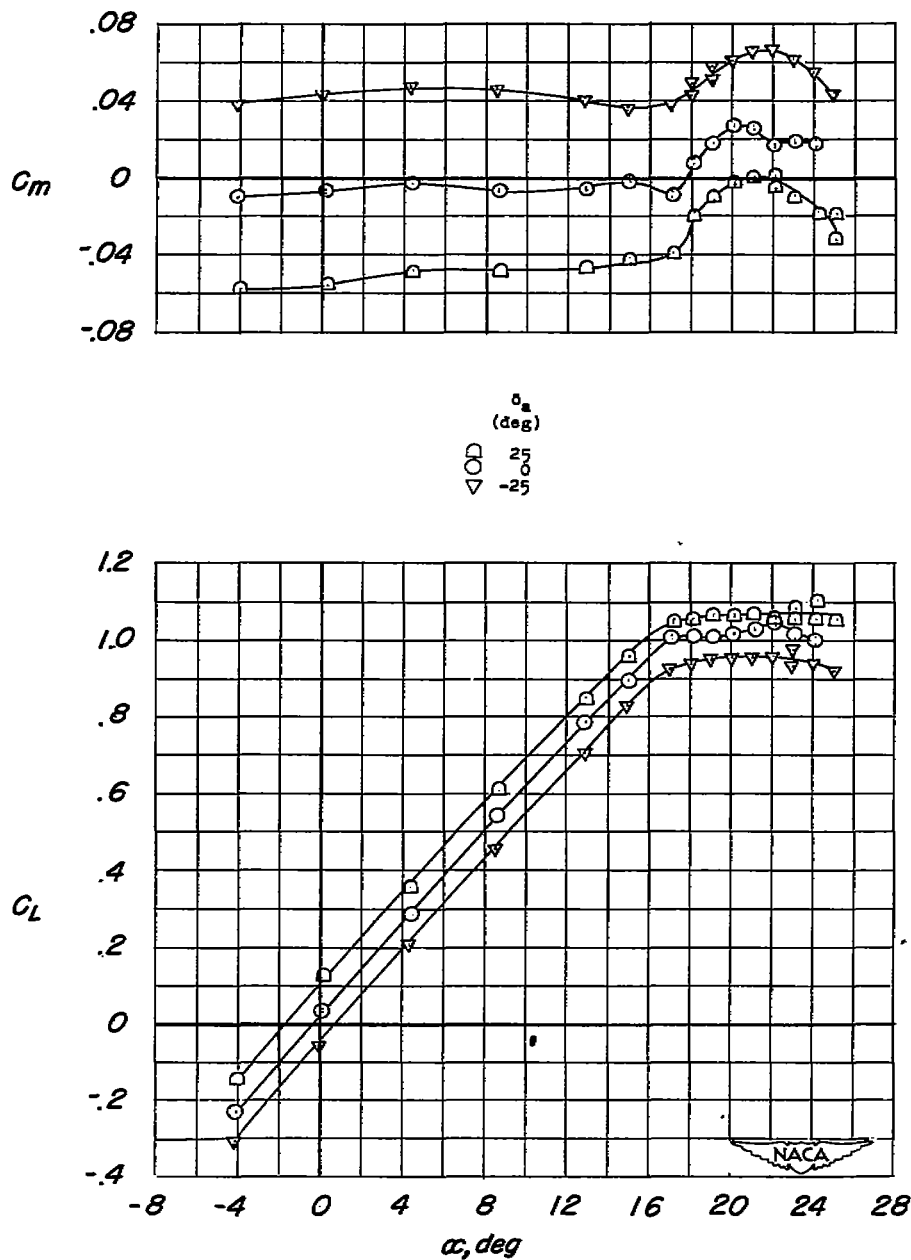
(a)  $C_{Z_\alpha}$ ,  $C_n$ , and  $C_l$  plotted against  $\alpha$ .

Figure 4.- Aileron characteristics of plain wing.



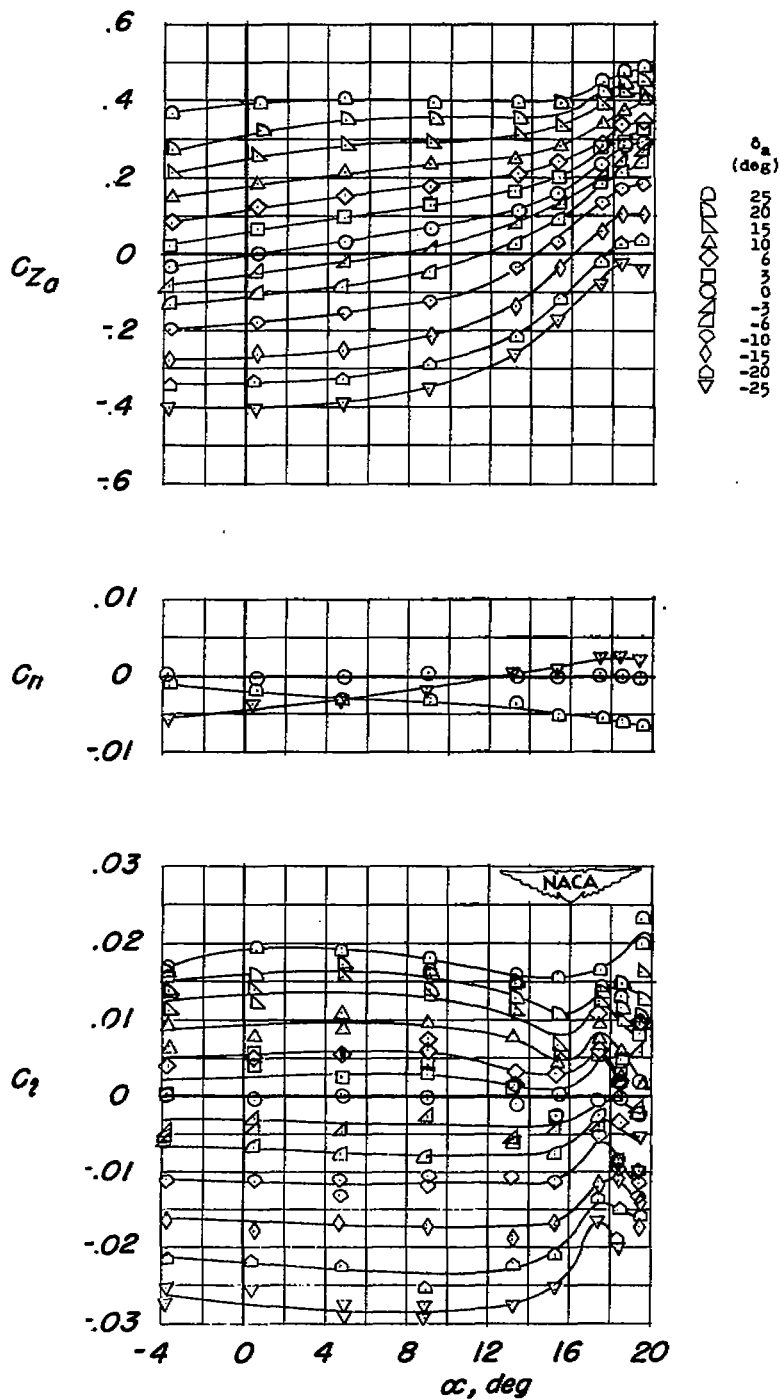
(b)  $P_R$  and  $C_{hta}$  plotted against  $\alpha$ .

Figure 4.- Continued.



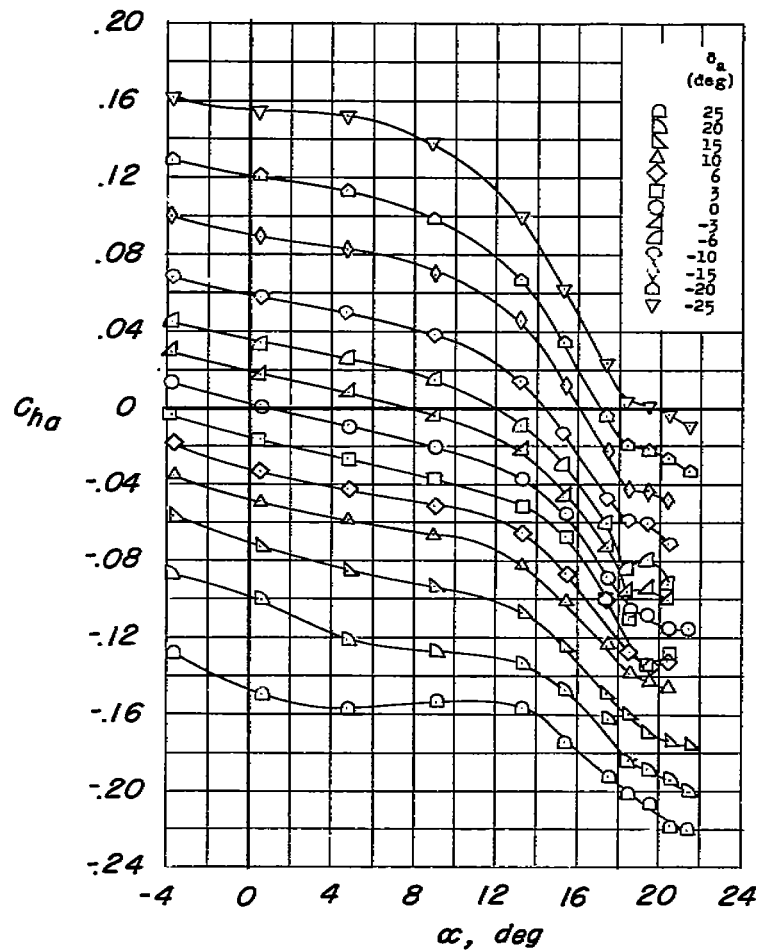
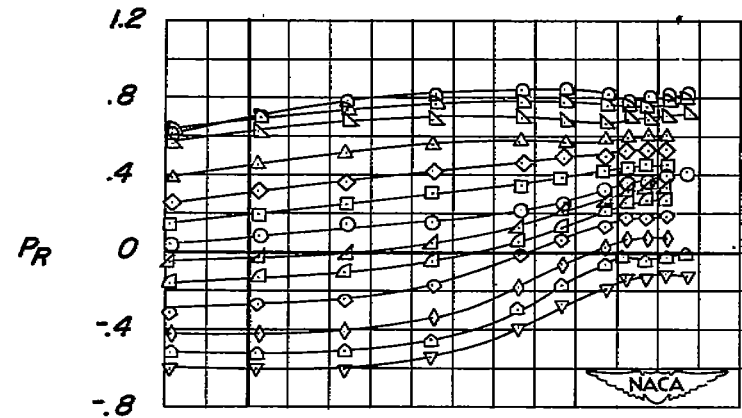
(c)  $C_m$  and  $C_L$  plotted against  $\alpha$ .

Figure 4.-- Concluded.



(a)  $C_{Z_a}$ ,  $C_n$ , and  $C_l$  plotted against  $\alpha$ .

Figure 5.- Aileron characteristics of wing with leading- and trailing-edge flaps deflected.



(b)  $P_R$  and  $C_{ha}$  plotted against  $\alpha$ .

Figure 5.- Continued.

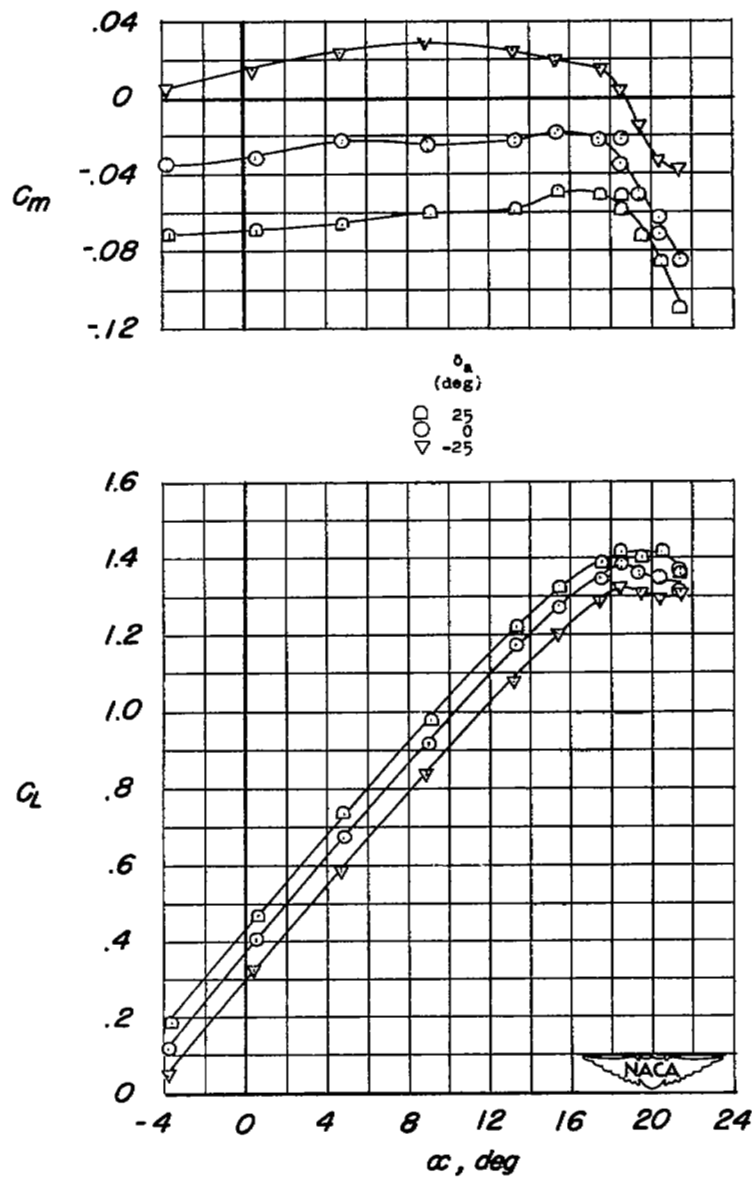
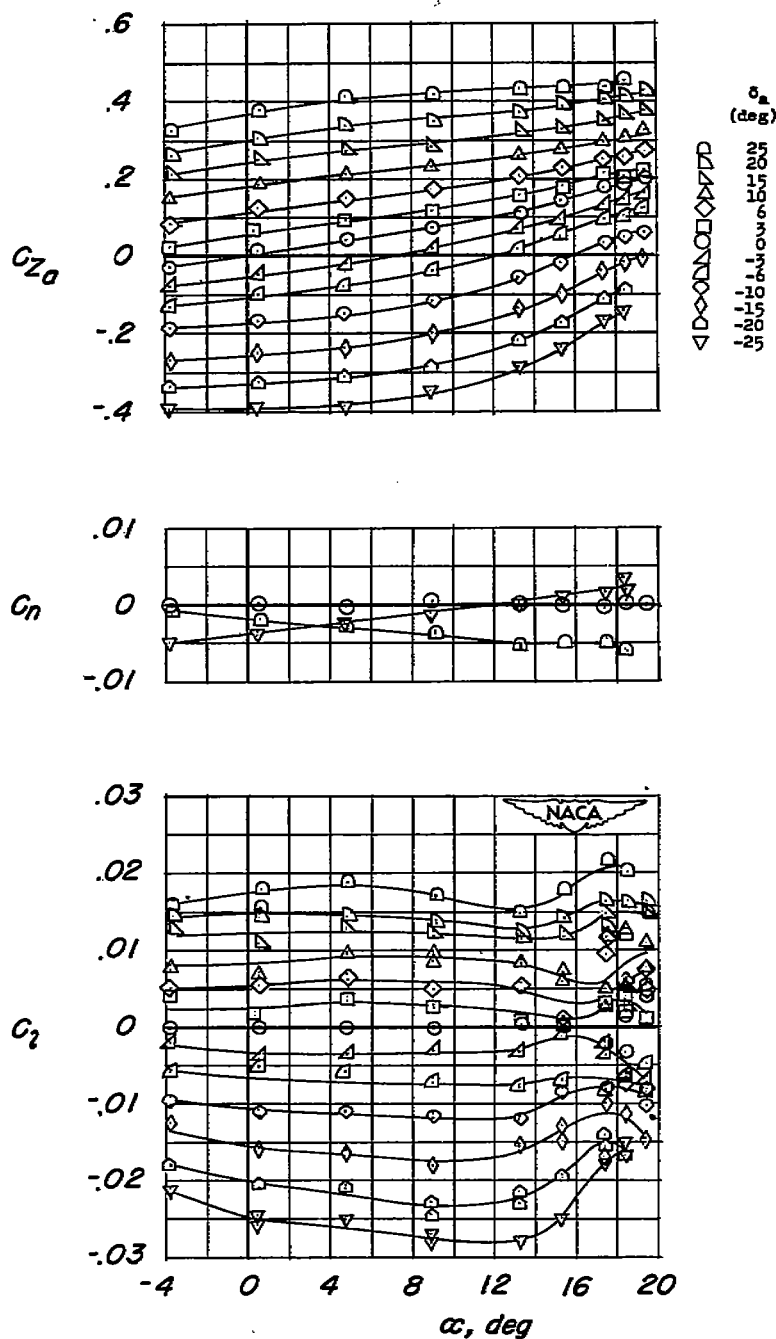
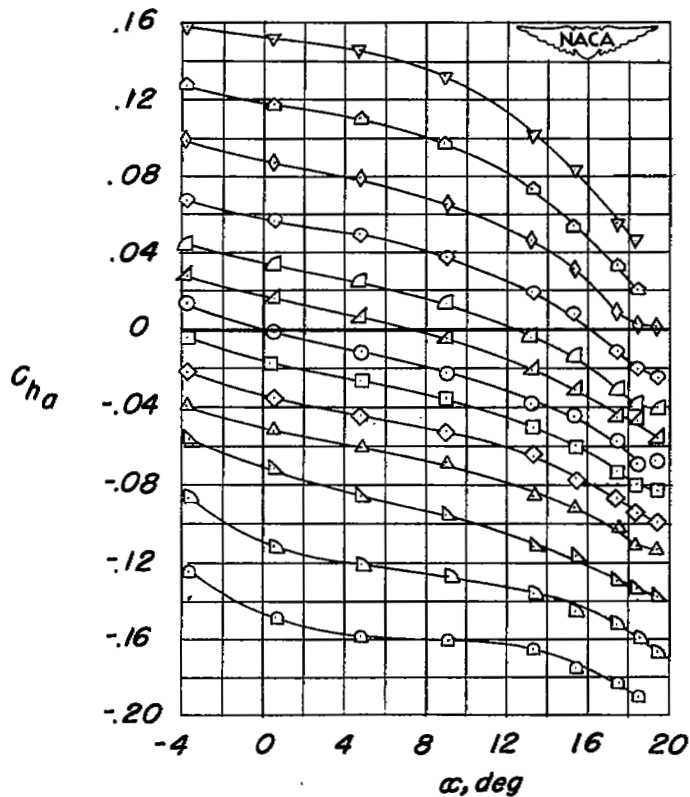
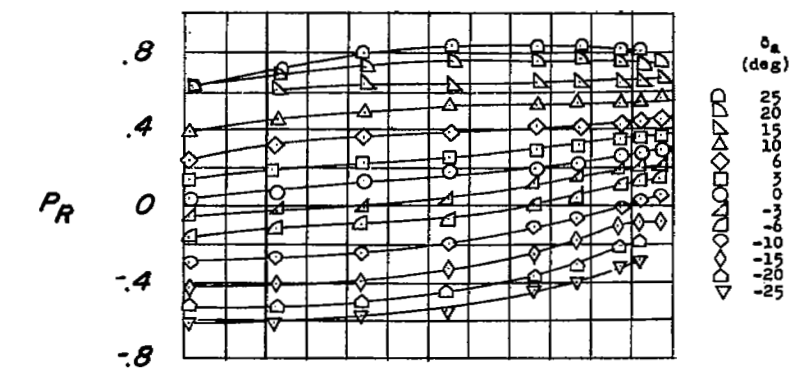
(c)  $C_m$  and  $C_L$  plotted against  $\alpha$ .

Figure 5.- Concluded.



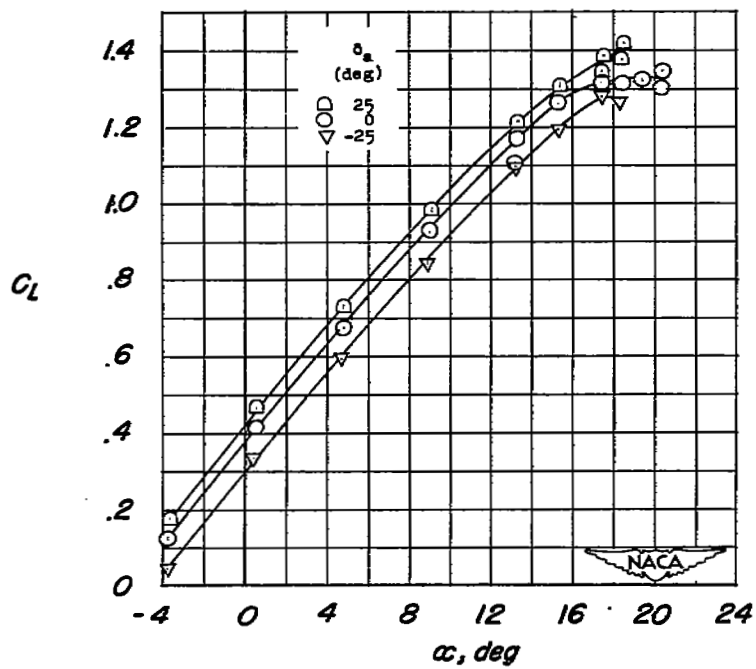
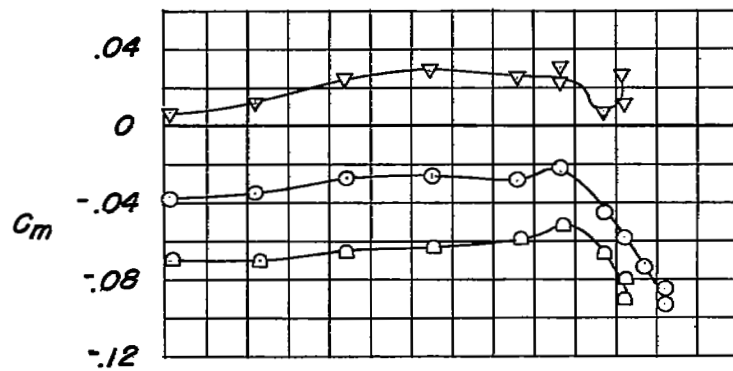
(a)  $C_{Z_a}$ ,  $C_n$ , and  $C_l$  plotted against  $\alpha$ .

Figure 6.— Aileron characteristics of wing with leading and trailing flaps deflected and fences installed.



(b)  $P_R$  and  $Ch_a$  plotted against  $\alpha$ .

Figure 6.- Continued.



(c)  $C_m$  and  $C_L$  plotted against  $\alpha$ .

Figure 6.- Concluded.

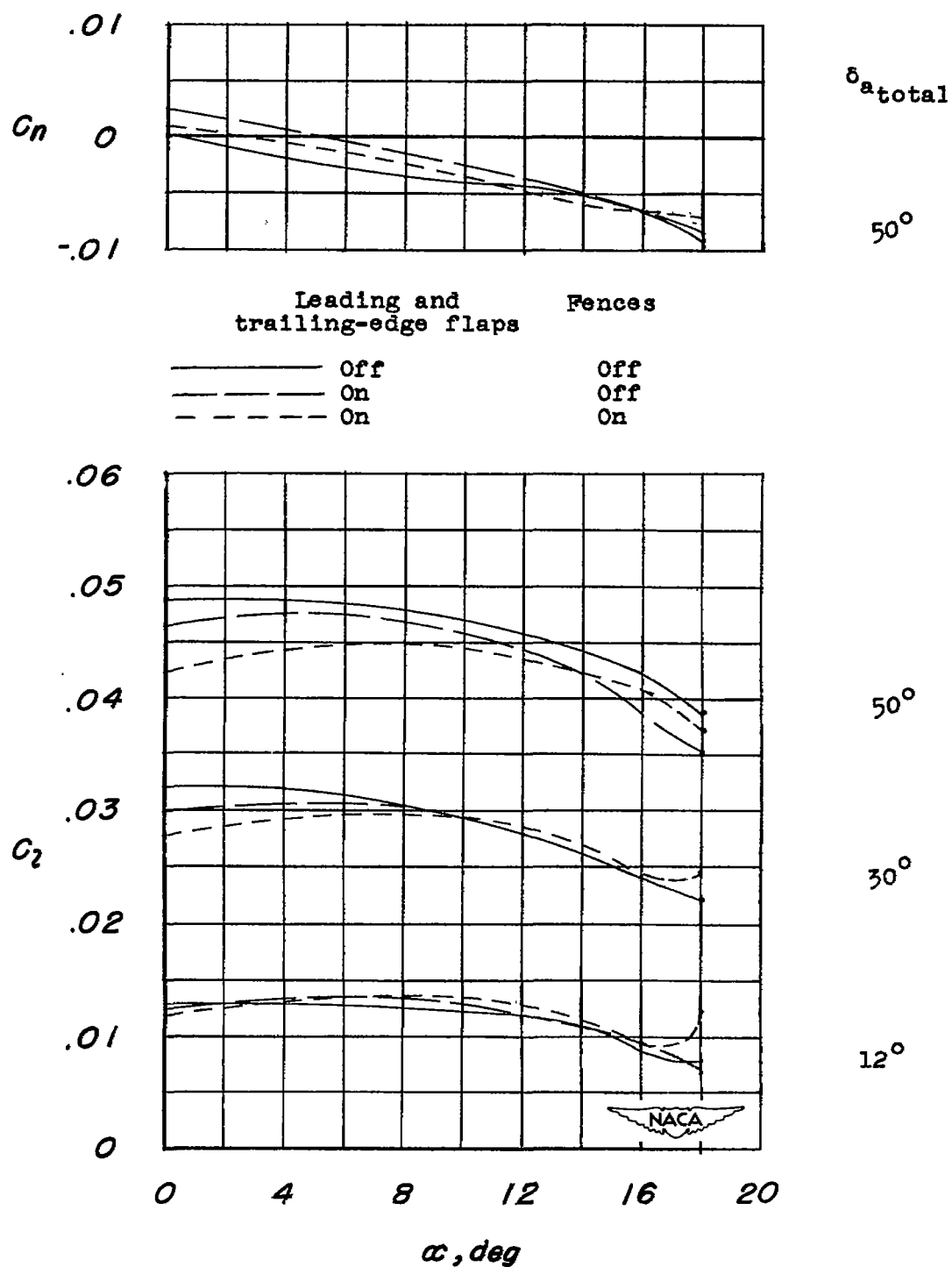


Figure 7.— Rolling-moment and yawing-moment characteristics for several model configurations and total aileron deflections.

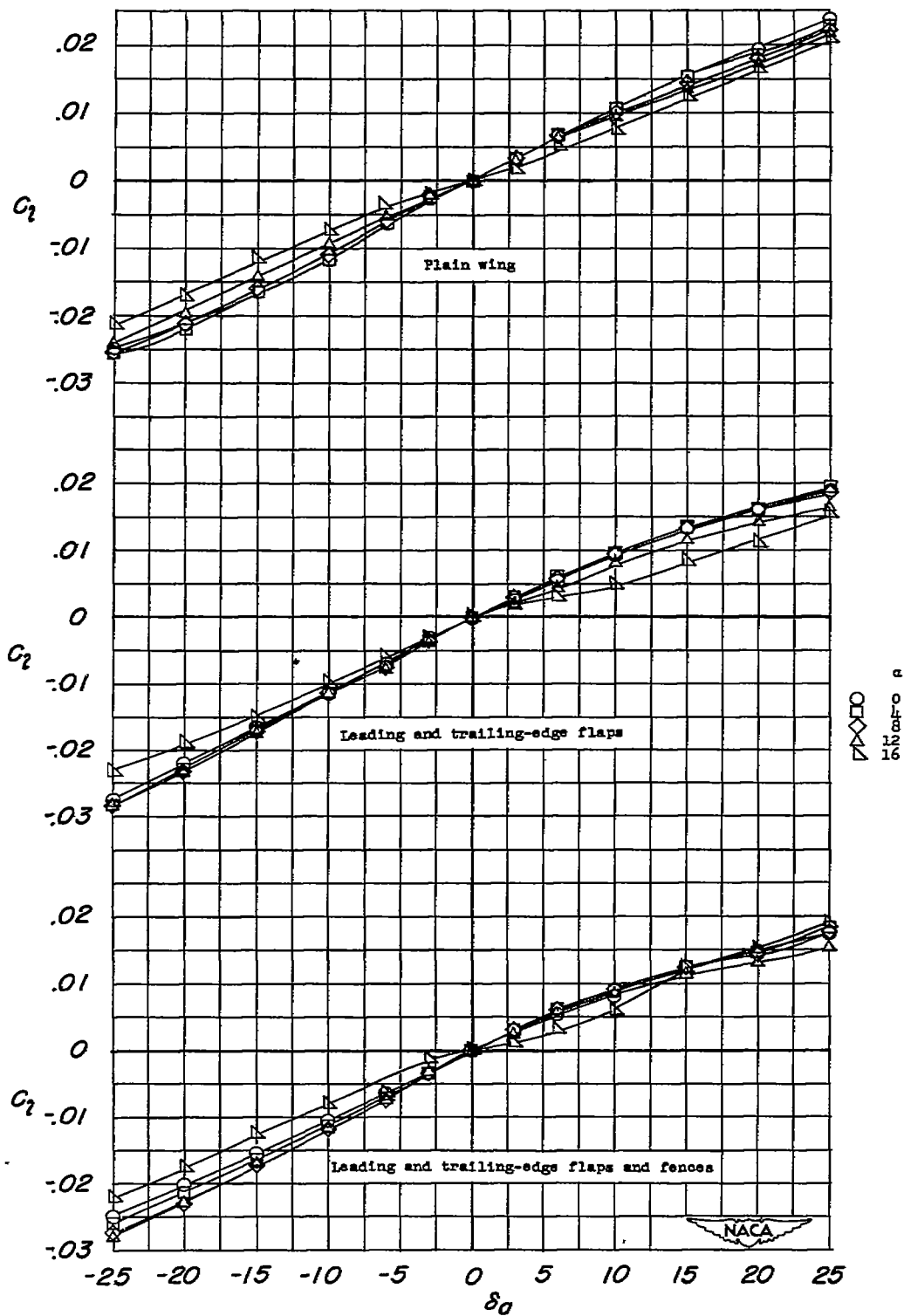


Figure 8.— The variation of rolling-moment characteristics with aileron deflection for various model configurations.

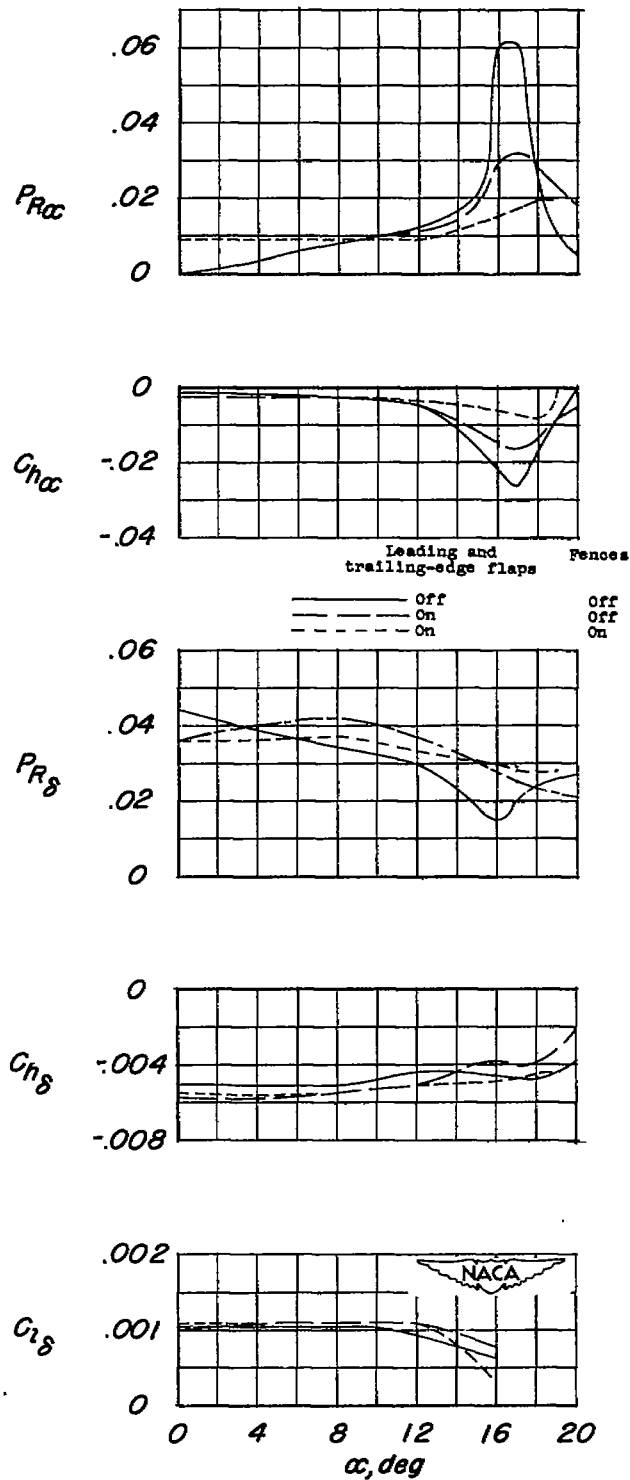


Figure 9.— The effects of high-lift and stall-control devices on the aileron hinge-moment and effectiveness parameters  $PR_{\alpha}$ ,  $CH_{\alpha}$ ,  $PR_{\delta}$ ,  $CH_{\delta}$ , and  $CL_{\delta}$ .

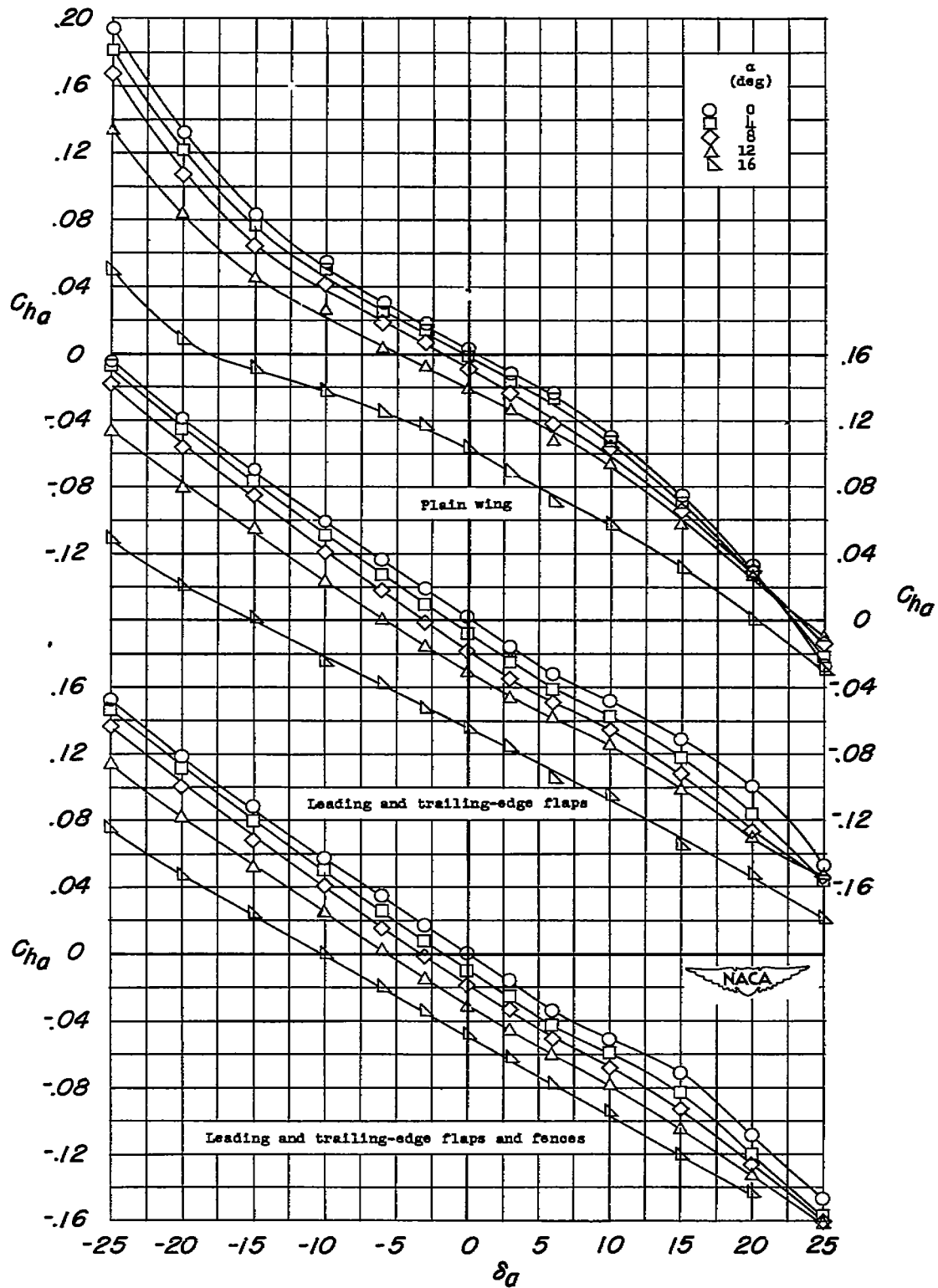


Figure 10.— The variation of aileron hinge-moment characteristics with aileron deflection for various model configurations.

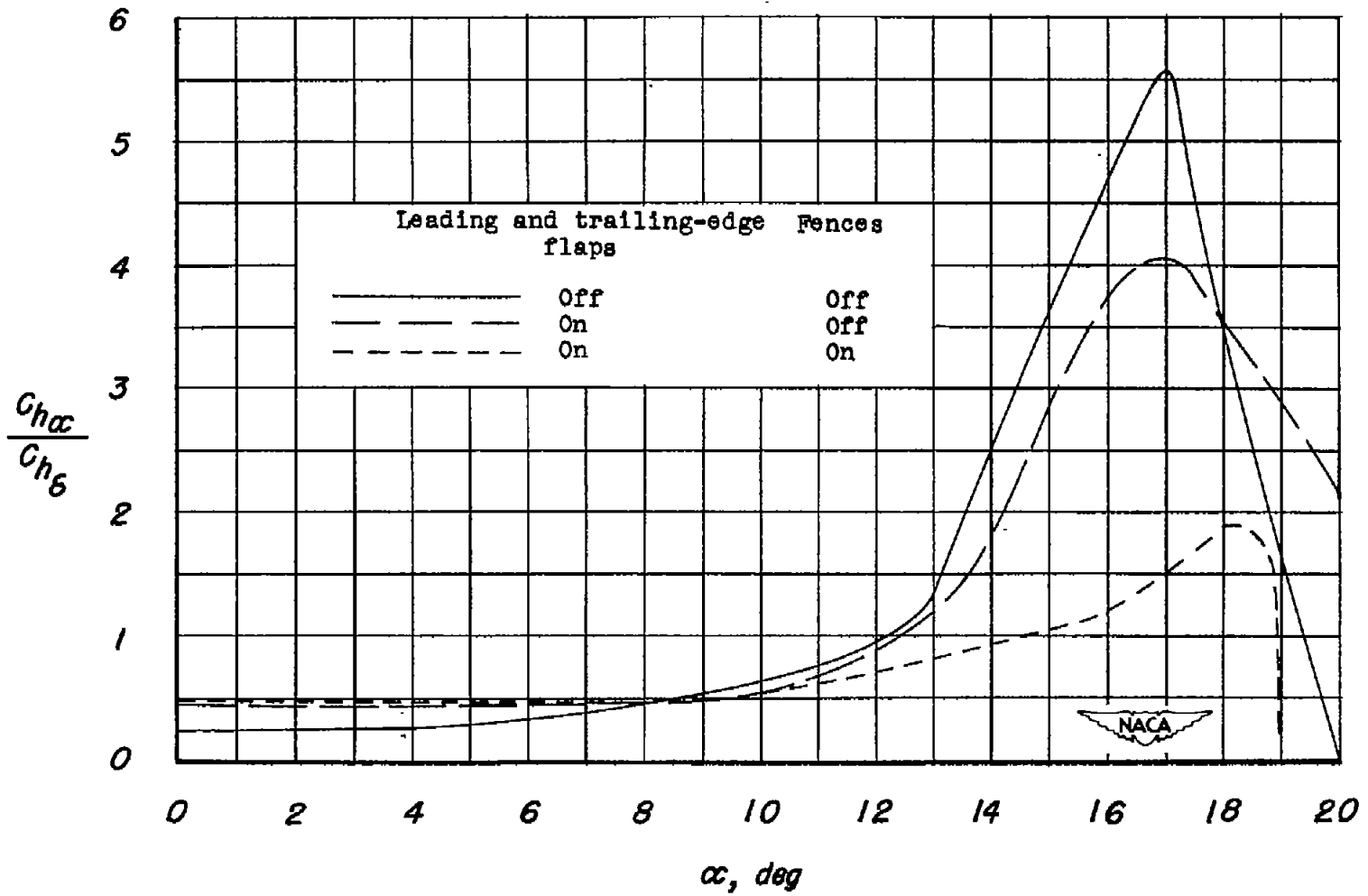


Figure 11.— The variation of  $C_{h\alpha}/C_{h\beta}$  with angle of attack for various model configurations.

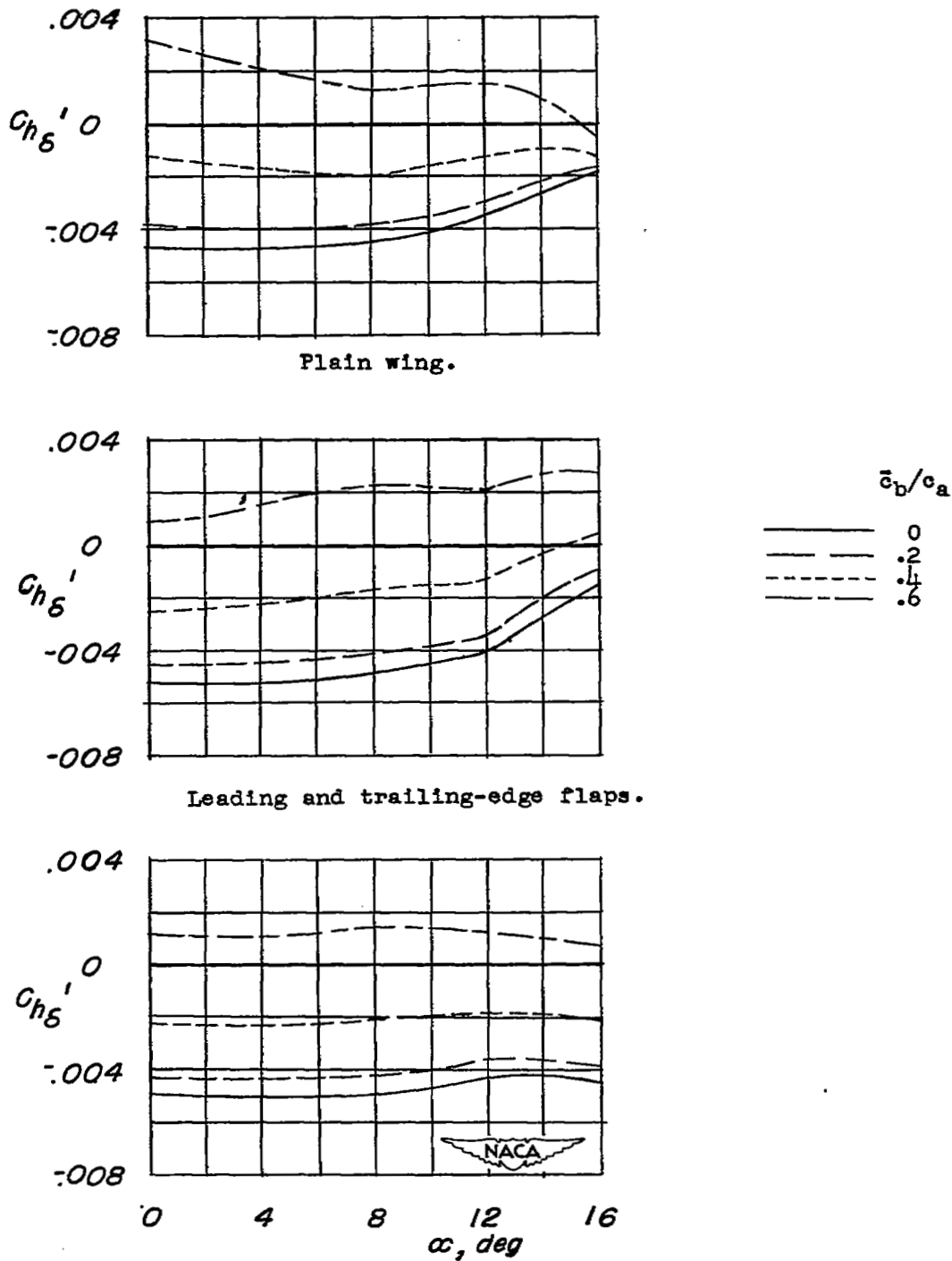


Figure 12.- The effect of various amounts of aerodynamic balance on the aileron hinge-moment parameter  $Ch_{\delta}'$ .

NASA Technical Library



3 1176 01436 7495